

## Supplementary Information

### Supplemental Methods

#### Identification of Structural Brain Hub Categories

*Hierarchical Clustering Analysis and Categories of Network Hubs.* To determine the suitable category number for the hierarchical clustering analysis (HCA), we performed the following analyses [Lange, et al., 2004; Yeo, et al., 2011]: a stability analysis to test the stability of the classification results across populations and a null-model analysis to assess the organizational uniqueness of the classification results for each classified category. In the first analysis, the group-averaged metric-to-metric spatial similarity matrix was initially computed by averaging the similarity matrices across all individuals, and the HCA classification results (i.e., 2 to 7 categories) of this matrix were referred to as the real assignment. Then, we randomly selected 5% of individuals to generate a new averaged similarity matrix and performed HCA to generate the classification results for this matrix using different category numbers (the bootstrapping assignment). For each category number, an instability value was estimated as the disagreement of the classification results between the real assignment and the bootstrapping assignment using the following formula [Lange, et al., 2004; Yeo, et al., 2011]:

$$E_c(\mathbf{BA}, \mathbf{RA}) = \min_{\mathbf{l} \in \mathbf{BA}} \frac{1}{N} \sum_{i=1}^N \delta(l_i \neq RA_i)$$

where  $E_c$  specifies the instability value of the category number  $c$ ,  $\mathbf{BA}$  represents all possible assigning labels for the bootstrapping assignment,  $\mathbf{RA}$  is one of the possible assigning labels for the real assignment,  $\mathbf{l}$  specifies one of the possible labels for the bootstrapping assignment,  $N$  is the number of graph-nodal metrics,  $l_i$  and  $RA_i$  are the assigning labels of metric  $i$  for the bootstrapping assignment and the real assignment, respectively, and  $\delta$  is denoted as 1 if  $l_i \neq RA_i$ , otherwise 0. This random sampling procedure was subsequently repeated 1000 times, which resulted in 1000 instability values for each category number. By comparing the instability values across different category numbers, we determined that the instability values for category numbers 2, 3 and 7 were significantly lower than those of the other category numbers (nonparametric permutation tests, 20000 times,  $P < 0.001$ , Bonferroni corrected, Fig. S1A), suggesting the clustering in these three situations was stable across populations.

Second, in the null model analysis, we assessed whether the spatial pattern among the classified categories was significantly different from the random situation. Briefly, for each individual, we initially estimated the metric-to-metric spatial similarity matrix and obtained the classification results under

categories 2 to 7 using HCA; these classifications were referred to as the individual assignment. One hundred corresponding random networks with the same size and degree distribution were subsequently generated for each individual and the metric classifications were similarly estimated as the random assignments. Thus, for each category number, the disagreement in the classification results between the individual assignment and each of the random assignments could be assessed using the previously described instability value formula and these instability values were further averaged for each individual to represent the differences in individual brain networks and the corresponding random situations. Finally, for each category number, we examined whether its averaged instability value was significantly higher than zero across individuals; with the exception of the use of 2 categories, the brain networks were significantly different from random situations (nonparametric permutation paired tests, 20000 times,  $P < 0.001$ , Bonferroni corrected, Fig. S1B). Collectively, both 3 and 7 categories corresponded to across-population stability and topological uniqueness of brain networks. Considering 7 categories are less meaningful, we classified the nodal metrics into 3 categories for further analyses.

### **R-fMRI Data Preprocessing**

The routine preprocessing of R-fMRI data was performed using DPABI [Yan, et al., 2016] for each participant. In detail, the first 5 volumes were removed, and the remaining volumes were corrected for slice timing and head motion. The T1-weighted image was co-registered to the mean functional image and was subsequently segmented into gray matter (GM), white matter (WM) and cerebrospinal fluid (CSF) using a unified segmentation algorithm. The resultant GM, WM and CSF images were further nonlinearly registered into the Montreal Neurological Institute (MNI) space with the transformation parameters estimated. Then, the functional data were normalized to the MNI space by using the estimated transformation parameters and resampled to 3-mm isotropic voxels. Next, spatial smoothing was applied to the normalized functional images with a 4-mm full width half maximum (FWHM) Gaussian kernel. The linear drift was subsequently detrended, and several nuisance signals, including the Friston's 24 head motion parameters, the signals from the whole brain, WM and CSF were regressed out to reduce respiratory and cardiac effects. Finally, temporal filtering (0.01 - 0.1 Hz) was performed on the time series of each voxel to reduce the effects of low-frequency drifts and high-frequency physiological noise.

### **R-fMRI Brain Network Analyses**

*Construction of Functional Brain Networks.* A group-level voxel-wise functional network (5% network density) was constructed based on the preprocessed R-fMRI data. Briefly, for each individual, we extracted the time series of each voxel within a GM mask, which was defined by thresholding the priori GM probabilistic template in SPM8 (GM probabilistic density > 0.2). The Pearson’s correlation of each pair of the time series was subsequently estimated, resulting in a functional connectivity matrix for each subject. Finally, we averaged the connectivity matrices across individuals to generate a grouped-averaged matrix and the top 5% strong connections were selected to define the group-level weighted functional network.

*Identification of Functional Brain Systems.* To examine the specificity of the distributions of structural hubs in functional systems, we identified the functional systems based on our group-level voxel-wise functional network. Briefly, we first applied a spectral community algorithm [Newman, 2006] to the functional network and 13 functional modules were identified (modules with a size less than 100 voxels were removed). According to previous functional connectome studies [Yeo, et al., 2011], we subsequently merged some of the 13 modules that were clearly sub-sets belonging to a large functional system, and obtained a seven-system parcellation that included the visual, sensorimotor, dorsal attention, ventral attention, limbic, frontoparietal and default-mode systems (Fig. S2A). Notably, our recent study demonstrated that network density likely affects the properties of voxel-wise functional networks [Du, et al., 2015]. Thus, we utilized two additional network densities (i.e., 1% and 10%) for modular identification. The adjusted mutual information [Vinh, et al., 2010] was used to quantify the similarity between every pair of modular structures. The results showed that the adjusted mutual information value was 0.571 between the 1%- and 5%-networks, 0.617 between the 5%- and 10%-networks, and 0.495 between the 1%- and 10%-networks, respectively. These results suggest a high similarity in modular structures among different network densities. Notably, there were no isolated nodes in any of the functional networks with different densities.

*Functional Participant Coefficients.* The functional participant coefficient quantifies the level that a given node connects to different functional systems [Hagmann, et al., 2008; He, et al., 2009; Power, et al., 2013]. We calculated the functional participant coefficient (FPC) for each node (i.e., voxel) in our group-level voxel-wise functional network using the following formula:

$$FPC_i = 1 - \sum_{s=1}^S (DC_{is}/DC_i)^2$$

3

where  $S$  is the number of functional modules,  $Dc_{is}$  specifies the degree of node  $i$  within module  $s$ , and  $Dc_i$  specifies the degree centrality of node  $i$  (Fig. S2B).

### **Investigating the Uniqueness of Hub Characteristics**

To determine whether the classification of nodal metrics and subsequent characterization results of the categorized hubs were unique in the brain networks or obtained by chance, we performed the following analyses. First, we generated all the possible combinations of clusters that had 4, 3, and 1 nodal metrics, which resulted in 280 groups with three categories of hub indices ( $C_8^4 \times C_4^3 \times C_1^1$ , 1 real combination and 279 surrogate combinations). Then, for each surrogate combination, we identified three categories of surrogate hubs (top 20%) and estimated their characteristics of microstructural organization, wiring cost, cognitive flexibility, functional association and topological vulnerability (a total of ten characteristics). Similar to our main analyses on miscellaneous characteristics, for each surrogate combination we performed statistical comparisons of these characteristics among the three categories of hubs. Finally, by applying the same statistical thresholds shown in Fig. 5, for a given surrogate combination we obtained the ranks of categorized hubs for each of ten characteristics; we subsequently determined whether the ranks in these surrogate combinations are consistent with those in the real combination. If one of characteristics is consistent, we called ‘match’ for this characteristic; otherwise, it was defined as ‘not match’. The proportions of surrogate combinations with 10, 9, 8, 7 and 6 characteristics that are consistent with the real one were subsequently estimated.

### **Validation Analysis**

To determine whether our findings are robust under different diffusion imaging protocols and fiber reconstructing algorithms, node definitions, hub selection thresholds, and consideration of isolated nodes, we implemented the validation analyses via four procedures:

*i) The Effects of Diffusion Imaging Protocol and Fiber Reconstructing Algorithm.* It has been argued that DTI tractography approaches may introduce false negative long-range connections and false positives in tracing between nearby regions because of their inaccuracies in resolving crossing fibers and tracts with sharp angles [Wedeen, et al., 2008]. Thus, to determine whether our main findings are insensitive to the diffusion imaging protocol and whether they are influenced by the fiber pathway reconstruction algorithm, we utilized the HARDI data from Dataset 3 to reconstruct individual structural brain networks with 1024 nodes. Specifically, we obtained the minimal preprocessing HARDI data with

eddy current and susceptibility distortion correction from the HCP website (<http://db.humanconnectome.org>) [Van Essen, et al., 2013]. The reconstruction of the diffusion profile was then implemented in a voxel-by-voxel manner using a generalized q-sampling imaging model [Yeh, et al., 2010]. Furthermore, whole-brain fiber tracts were generated, and individual structural networks were constructed. Finally, we identified the hub categories and examined their spatial distributions and miscellaneous characteristics.

*ii) The Effects of Node Definition of the Structural Network.* Previous studies have demonstrated that different node definitions used during brain network construction may lead to differences in network topological properties [Wang, et al., 2009; Zalesky, et al., 2010]. Using Dataset 1, we validated whether our main findings were affected by another regional parcellation with 625 nodes that were generated based on the constraint of the anatomical transcendental boundaries of automated anatomical labeling. Network construction and analyses were performed again, as previously described. **In addition, there were some anatomical overlaps across different hubs (e.g. posterior cingulate cortex), which might due to the adoption of high resolution 1024-node parcellation. Therefore, we utilized a coarser 360-node multi-modal parcellation [Glasser, et al., 2016] to validate our findings on Dataset 3.**

*iii) The Effects of Hub Selection Thresholds.* In this study, the brain nodes with the top 20% of hub indices were defined as hubs, which may influence our conclusions. Therefore, based on Dataset 1, we also selected two additional thresholds, the top 15% and the top 25% of hub indices, to define brain hubs. The hub characteristics were explored again to verify our main findings.

*iv) The Effects of Isolated Nodes.* To examine whether hub classification and identification were sensitive to the existence of isolated nodes in the brain networks, we performed the following analyses in Dataset 1. Briefly, we first calculated the percentage of isolated nodes for each individual network. Then, for each node, the probability of isolation was calculated across individuals, resulting in a probabilistic map of isolated nodes at the group-level. Finally, we calculated the nodal metrics on the individual networks with the removal of isolated nodes and re-performed the hierarchical clustering analysis to identify categorized hubs.

*v) The Effects of Modular Organization for calculating participant coefficient.* In our main analysis, the participant coefficient was calculated based on the modular organization specifically estimated for each subject. To validate whether estimating the modular organization at different levels (i.e., individual-level

or group-level) could affect the distribution of the participant coefficient, we re-calculated the participant coefficients according to a group-level modular organization. In detail, we first created a group-level binary network by selecting all connections that were present in at least 25.34% of the group of individuals (this threshold ensured the same sparsity as the mean of individual networks). Then, we implemented the spectral community algorithm [Newman, 2006] for this group-level network and obtained the group-level modular organization. Finally, for each subject we estimated the individual participant coefficient map according to this group-level modular organization and subsequently re-performed our analyses.

### **Statistical Analysis**

Unless specifically noted, all comparisons involving between-systems, hubs vs. non-hubs, and among three categories of hubs were performed using paired nonparametric permutation tests across individuals. Briefly, for each pair of samples, the difference of the mean values between two paired sample groups (e.g., the mean difference of the FA between the aggregated hubs and non-hubs across subjects, or the mean difference of the streamline cost between the aggregated hubs and the distributed hubs across subjects) was initially calculated. For each permutation, the paired samples were randomly interchanged between two groups and the mean difference between groups was then re-computed. A total of 20,000 permutations were performed to generate an empirical distribution of the difference. Furthermore, the original difference between two paired sample groups was assigned a  $P$  value as the proportion of random values in the obtained empirical distribution. The 95<sup>th</sup> percentile point of the empirical distribution was used as a critical value in a one-tailed test to determine whether the observed group differences could occur by chance. Notably, the usage of 20,000 permutations ensures that the minimum uncorrected  $P$ -value obtained from the permutation test can fulfill the condition of the Bonferroni correction.

### **Supplemental Results**

#### **Validation Results**

*Data using Different Imaging and Tractography Protocols.* We validated the main findings by re-performing our analysis on Dataset 3 (HARDI data from HCP). We found remarkably similar or different spatial distributions between specific network nodal metrics (range of Spearman's  $\rho$ : 0.29~1.00), which were highly similar to the main results (Fig. S6A and 3A). The HCA classified the eight nodal metric maps into three categories: i) eigenvector centrality, subgraph centrality, K-core

centrality, closeness centrality, and degree centrality; ii) betweenness centrality and page-rank centrality; and ii) participant coefficient (Fig. S6A). Of note, degree centrality was classified into the first category, which may suggest the bipolar topological character of degree centrality and/or its potential sensitivity to different diffusion imaging protocols or fiber reconstructing algorithms. Although the classification result was slightly changed, the spatial distributions of all three hub indices over the whole brain and within functional systems were nearly the same as the main findings; moreover, the commonly identified hub nodes in all three categories were primarily located at the default-mode system ( $P$ -values  $< 0.005$ , Bonferroni corrected) with additionally identified hub nodes in the visual system for aggregated hubs and in the sensorimotor and ventral attention systems for connector-hubs ( $P$ -values  $< 0.01$ , Bonferroni corrected) (Fig. S6B and S6C). Moreover, all three categories of hubs exhibited better microstructural organization, greater wiring costs, higher functional associations, more cognitive flexibility and heavier topological vulnerability than non-hubs ( $P$ -values  $< 0.001$ , Bonferroni corrected). Among the three categories of hubs, the aggregated hubs exhibited the largest generalized FA values and the longest streamline length, the distributed hubs exhibited the highest streamline cost and topological vulnerability, and the connector hubs exhibited the strongest functional association and highest cognitive flexibility ( $P$ -values  $< 0.001$ , Bonferroni corrected) (Fig. S7). These results indicate the strong reproducibility of our findings under different imaging and tractography methods.

*625-Node Definition.* We used a 625-node constrained-random parcellation to re-construct the whole-brain WM individual networks (based on Dataset 1) and found that the results were largely consistent with our results in the main text. Briefly, the classification of the three categories of metrics was exactly the same as the classification used in the main text, and the spatial patterns and system distributions of the hub indices were largely consistent with the main results (Fig. S8). Moreover, the distinct miscellaneous characteristics of different structural brain hubs were extremely retained, which were highly similar to those of the networks with 1024 nodes (for all comparisons of characteristics between hubs and non-hubs and among three categories of hubs,  $P$ -values  $< 0.001$ , Bonferroni corrected) (Fig. S9). Collectively, our main findings were independent of the node definition during structural brain network construction.

*360-Node Definition.* We adopted a 360-node multi-modal parcellation to re-identify the three categories of hubs and examined their spatial distribution (based Dataset 3). The spatial distributions of three categories of hubs were largely consistent with our main findings except that the closeness centrality

was classified into the category of distributed hub (Fig. S10). Overlapped regions are mainly distributed in the posterior cingulate cortex, medial prefrontal cortex, temporal pole and visual cortex, particularly in the default-mode system (Fig. S10B and S10C). These results indicate that our main findings were stable regardless of the resolutions of brain parcellations.

*Thresholds for Hub Identification.* The nodes with the top 20% of hub indices were identified as the hubs in the main analysis, and two additional thresholds, 15% and 25%, were used for validation analyses. We found that under the threshold of 15% (Fig. S11) or 25% (Fig. S12), all three categories of hubs exhibited better microstructural organization, greater wiring costs, higher functional association, more cognitive flexibility and heavier topological vulnerability than non-hubs, and the diversity of these characteristics among brain hubs was highly consistent with the main findings (for all comparisons of characteristics between hubs and non-hubs and among three categories of hubs,  $P$ -values  $< 0.001$ , Bonferroni corrected).

*Spatial Distribution of Isolated Nodes and Their Influences on Classification of Nodal Metrics.* The results showed that only a few nodes were isolated in the individual networks (percentages:  $5.4\% \pm 1.8\%$  nodes; range: 1.7%~11.2% nodes). The majority of the isolated nodes (group-level probability  $> 25\%$ ) were mainly located near the midline and lateral regions of the brain (Fig. S13A). Here, the probability threshold, 25%, corresponded to the top 60 nodes, which was comparable to the mean number of isolated nodes across subjects (i.e., 55.7 nodes) (Fig. S13B). The results with the removal of isolated nodes were not different from our main findings (Figs. 3A and S13C), implying that our main findings were not affected by the removal of isolated nodes or not.

*Calculation of Participant Coefficient Using Group-level Modular Organization.* We repeated our main analyses which were performed on Dataset 1 with the participant coefficient defined by group-level modular organization. The classification of eight nodal metrics was consistent with the corresponding results in the main text (Fig. S3A and S14A). The spatial distributions of the connector hub indices derived from group- and individual-level modular organization were significantly similar ( $\rho = 0.4682$ ,  $P$ -value =  $6.34 \times 10^{-57}$ ; Fig. S14B), and the spatial distributions of the connector hub indices within functional systems were nearly the same as our main findings (Fig. 4B and S14C). All three categories of hubs exhibited better microstructural organization, greater wiring costs, higher functional association, more cognitive flexibility and heavier topological vulnerability than non-hubs ( $P$ -values  $< 0.001$ , Bonferroni corrected, Fig. S15A). Moreover, among the three categories of hubs, the aggregated hubs

exhibited the largest FA values and the longest streamline length, the distributed hubs exhibited the highest streamline cost and topological vulnerability, and the connector hubs exhibited the strongest functional association and highest cognitive flexibility ( $P$ -values < 0.001, Bonferroni corrected) (Fig. S15B). These results indicate that our findings are stable when calculating participant coefficients regardless of using group-level or individual-level modular organizations.

## References

- Alvarez-Hamelin, J.I., Dall'Asta, L., Barrat, A., Vespignani, A. (2006) Large scale networks fingerprinting and visualization using the k-core decomposition. In: Weiss, Y., Scholkopf, B., Platt, J., editors. *Adv. Neural. Inf. Process. Syst.* Cambridge (Massachusetts): MIT Press. p 41-50.
- Boldi, P., Santini, M., Vigna, S. (2009) PageRank: functional dependencies. *ACM Trans. Inf. Syst.*, 27:1-23.
- Bonacich, P. (1972) Factoring and weighting approaches to status scores and clique identification. *J. Math. Sociol.*, 2:113-120.
- Bonacich, P. (1991) Simultaneous group and individual centralities. *Soc. Networks*, 13:155-168.
- Du, H., Liao, X., Lin, Q., Li, G., Chi, Y., Liu, X., Yang, H., Wang, Y., Xia, M. (2015) Test-retest reliability of graph metrics in high-resolution functional connectomics: a resting-state functional MRI study. *CNS Neurosci. Ther.* , 21:802-816.
- Estrada, E., Rodriguez-Velazquez, J.A. (2005) Subgraph centrality in complex networks. *Phys. Rev. E.*, 71:056103.
- Freeman, L.C. (1978) Centrality in social networks conceptual clarification. *Soc. Networks*, 1:215-239.
- Freeman, L.C. (1980) The gatekeeper, pair-dependency and structural centrality. *Qual. Quant.*, 14:585-592.
- Glasser, M.F., Coalson, T.S., Robinson, E.C., Hacker, C.D., Harwell, J., Yacoub, E., Ugurbil, K., Andersson, J.L., Beckmann, C.F., Jenkinson, M., Smith, S.M., Van Essen, D.C. (2016) A multi-modal parcellation of human cerebral cortex. *Nature*, 536:171-178.
- Hagmann, P., Cammoun, L., Gigandet, X., Meuli, R., Honey, C.J., Wedeen, V.J., Sporns, O. (2008) Mapping the structural core of human cerebral cortex. *PLoS Biol.* , 6:e159.
- He, Y., Wang, J., Wang, L., Chen, Z.J., Yan, C., Yang, H., Tang, H., Zhu, C., Gong, Q., Zang, Y., Evans, A.C. (2009) Uncovering intrinsic modular organization of spontaneous brain activity in humans. *PLoS ONE*, 4:e5226.
- Katz, L. (1953) A new status index derived from sociometric analysis. *Psychometrika*, 18:39-43.
- Lange, T., Roth, V., Braun, M.L., Buhmann, J.M. (2004) Stability-based validation of clustering solutions. *Neural. Comput.*, 16:1299-1323.
- Newman, M.E. (2006) Modularity and community structure in networks. *Proc. Natl. Acad. Sci. U. S. A.*, 103:8577-8582.

- Page, L., Brin, S., Motwani, R., Winograd, T. 1999. The PageRank citation ranking: bringing order to the web. Stanford InfoLab.
- Power, J.D., Schlaggar, B.L., Lessov-Schlaggar, C.N., Petersen, S.E. (2013) Evidence for hubs in human functional brain networks. *Neuron*, 79:798-813.
- Van Essen, D.C., Smith, S.M., Barch, D.M., Behrens, T.E., Yacoub, E., Ugurbil, K., the WU-Minn HCP Consortium. (2013) The WU-Minn human connectome project: an overview. *NeuroImage*, 80:62-79.
- Vinh, N.X., Epps, J., Bailey, J. (2010) Information Theoretic Measures for Clusterings Comparison: Variants, Properties, Normalization and Correction for Chance. *J. Mach. Learn. Res.*, 11:2837-2854.
- Wang, J., Wang, L., Zang, Y., Yang, H., Tang, H., Gong, Q., Chen, Z., Zhu, C., He, Y. (2009) Parcellation-dependent small-world brain functional networks: a resting-state fMRI study. *Hum. Brain Mapp.*, 30:1511-1523.
- Wedeen, V.J., Wang, R., Schmahmann, J.D., Benner, T., Tseng, W., Dai, G., Pandya, D., Hagmann, P., D'Arceuil, H., de Crespigny, A.J. (2008) Diffusion spectrum magnetic resonance imaging (DSI) tractography of crossing fibers. *NeuroImage*, 41:1267-1277.
- Yan, C.G., Wang, X.D., Zuo, X.N., Zang, Y.F. (2016) DPABI: Data Processing & Analysis for (Resting-State) Brain Imaging. *Neuroinformatics*, 14:339-351.
- Yeh, F.C., Wedeen, V.J., Tseng, W.Y.I. (2010) Generalized-sampling imaging. *IEEE Trans. Med. Imaging* 29:1626-1635.
- Yeo, B.T., Krienen, F.M., Sepulcre, J., Sabuncu, M.R., Lashkari, D., Hollinshead, M., Roffman, J.L., Smoller, J.W., Zöllei, L., Polimeni, J.R., Fischl, B., Liu, H., Buckner, R.L. (2011) The organization of the human cerebral cortex estimated by intrinsic functional connectivity. *J. Neurophysiol.*, 106:1125-1165.
- Zalesky, A., Fornito, A., Harding, I.H., Cocchi, L., Yücel, M., Pantelis, C., Bullmore, E.T. (2010) Whole-brain anatomical networks: does the choice of nodes matter? *NeuroImage*, 50:970-983.
- Zuo, X.N., Ehmke, R., Mennes, M., Imperati, D., Castellanos, F.X., Sporns, O., Milham, M.P. (2012) Network centrality in the human functional connectome. *Cereb. Cortex*, 22:1862-1875.

## Supplemental Tables

**Table S1.** Detailed description of eight graph nodal metrics

Nodal Metric Name (Abbreviation)	Description	Formula	Annotation
Betweenness Centrality (Bc)	Freeman's betweenness centrality specifies the number of times that a node is on the shortest path between two other nodes in network [Freeman, 1980].	$BC_k = \sum_{i=1}^N \sum_{j=1}^N g_{ikj} / g_{ij}$	$N$ is the number of nodes, $g_{ikj}$ is the number of shortest paths between node $i$ and node $j$ passing through node $k$ , and $g_{ij}$ is the total number of all shortest paths between node $i$ and node $j$ .
Closeness Centrality (Cc)	Freeman's normalized closeness centrality is defined as the reciprocal of averaged distance across all shortest paths between a given node and the other nodes [Freeman, 1978].	$CC_i = (N - 1) / \sum_{j=1}^N (d_{ij})$	$N$ is the number of nodes, and $d_{ij}$ is the length of shortest path between node $i$ and node $j$ .
Degree Centrality (Dc)	Degree centrality is calculated as the number of edges connected to a given node [Freeman, 1978].	$DC_i = \sum_{j=1}^N A_{ij}$	$N$ is the number of nodes, and $A$ is the adjacent matrix, if there is an edge between node $i$ and node $j$ , $A_{ij} = 1$ , otherwise $A_{ij} = 0$ .
Eigenvector Centrality (Ec)	Eigenvector centrality is the principal eigenvector of the adjacency matrix [Bonacich, 1972]. In particular, it mathematically equivalent to Katz's centrality [Katz, 1953] as the damping factor approaches the reciprocal of the principal eigenvalue from below [Bonacich, 1991], and it is the weighted count of all walks for a	$EC_i = \mu_i^{1-\alpha} \sum_{j=1}^N \sum_{k=1}^{+\infty} (1/\lambda_1)^k (A^k)_{ij}$	$N$ is the number of nodes, $\mu_i^1$ is the $i$ th component of the principal eigenvector, $\lambda_1$ is the largest eigenvalue of the adjacency matrix, $A$ is the adjacent matrix, and $(A^k)_{ij}$ specifies the path between node $i$ and node $j$ with $k$ step walking.

	given node that considers indirect paths.		
K-core Centrality (Kc)	K-core decomposition assigns a set of nodes to $k$ if and only if the minimum degree of the subgraph comprised of these nodes is $k$ [Alvarez-Hamelin, et al., 2006]. It assesses the level of interconnection between each other for a given set of nodes [Hagmann, et al., 2008].	$G = (V, E),$ $H = (C, E C), C \subseteq V,$ $\forall v \in C, Dc_v \geq k,$ $Kc_C = k$	$G$ represents a graph, $V$ is the node set, $E$ is the edge set, $H$ is the subgraph, $v$ is a given node in subgraph $H$ , $Dc_v$ specifies the degree centrality of node $v$ .
Participant Coefficient (Pc)	Participant coefficient quantifies the level that a given node connects to different network modules [Hagmann, et al., 2008; He, et al., 2009; Power, et al., 2013].	$Pc_i = 1 - \sum_{s=1}^S (Dc_{is}/Dc_i)^2$	Where, $S$ is the number of modules, $Dc_{is}$ specifies the number of edges between node $i$ and the other nodes within module $s$ , and $Dc_i$ specifies the degree centrality of node $i$ .
Page-rank Centrality (Pr)	Google's page-rank centrality [Page, et al., 1999] is a variant of the eigenvector centrality [Zuo, et al., 2012]. The damping factor was set to 0.85, which was generally used in previous studies and introduced a small probability walking on the graph [Boldi, et al., 2009].	$Pr_i = (1 - d)/N + d \sum_{j=1}^N (A_{ij}/Dc_i)$	$N$ is the number of nodes, $d$ is the damping factor, $A$ is the adjacent matrix, and $Dc_i$ specifies the degree centrality of node $i$ .
Subgraph Centrality (Sc)	Subgraph centrality [Estrada and Rodriguez-Velazquez, 2005] quantifies the number of subgraphs in which a given node is included.	$Sc_i = \sum_{k=0}^{+\infty} (A^k)_{ii}/k! = \sum_{j=1}^N \mu_{ij}^2 e^{\lambda_j}$	$(A^k)_{ii}$ is the number of subgraphs with $k$ step walking, $\mu_{ij}$ is the $i$ th component of $j$ th eigenvector, and $\lambda_j$ specifies $j$ th eigenvalue of the adjacent matrix $A$ .

## Supplemental Figures

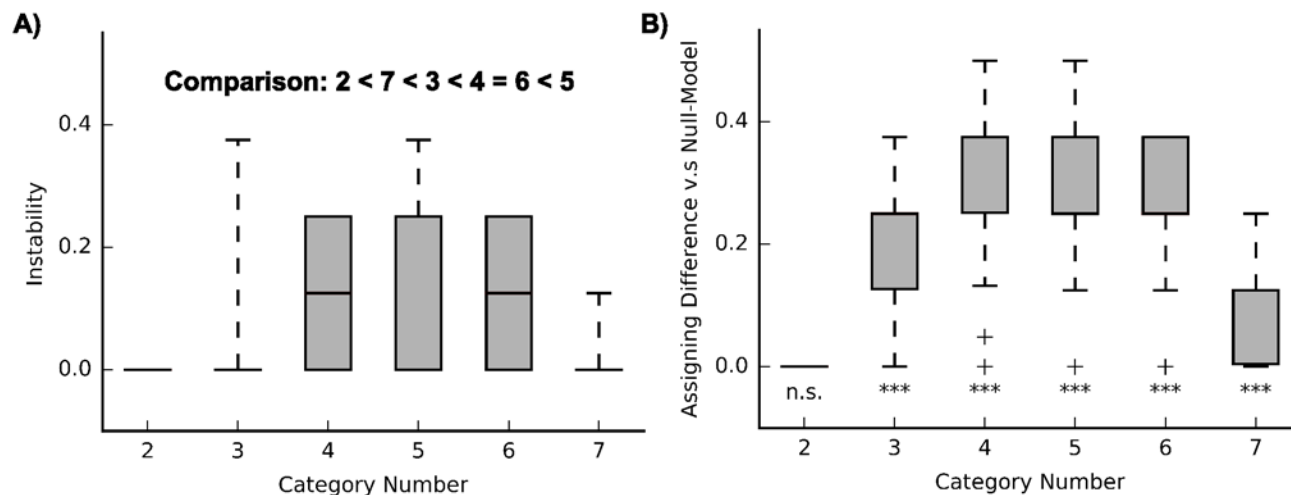


**Figure S1. Identification of the Category Number of the Hierarchical Clustering Analysis.** (A) The instability of classification with different category numbers. The symbol “<” indicates that the item to the left is significantly lower than the item to the right ( $P < 0.001$ , Bonferroni corrected), and the symbol “=” represents no significant differences between the left and right items. (B) The assigning differences compared with null models when using different category numbers. The symbol “\*\*\*” indicates that the assigning difference is significantly larger than 0 ( $P < 0.001$ , Bonferroni corrected), and the symbol “n.s.” indicates non-significant.

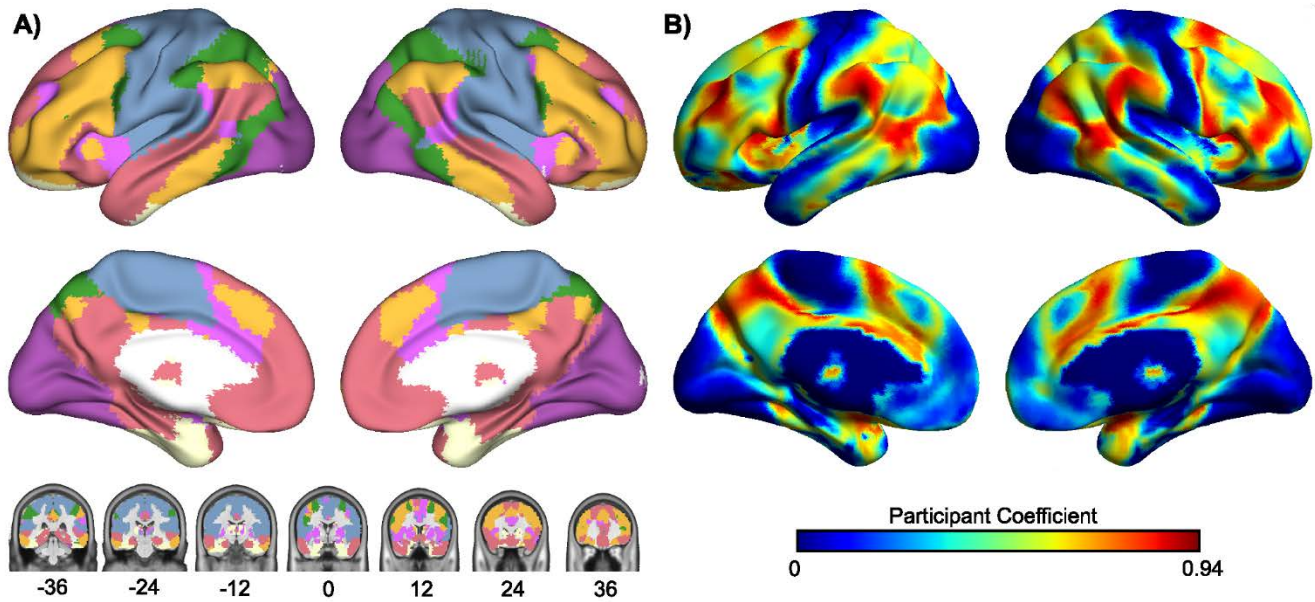


**Figure S2. Brain Functional Systems and Functional Participant Coefficient.** (A) Seven functional systems identified using the fMRI data in Dataset 1. These functional systems were mapped to a brain surface and 8 coronal slices (subcortical regions: MNI coordinates from  $y = -36$  to  $36$  with steps of  $12$  mm). (B) The corresponding functional participant coefficient distribution of the group-level voxel-wise functional network.

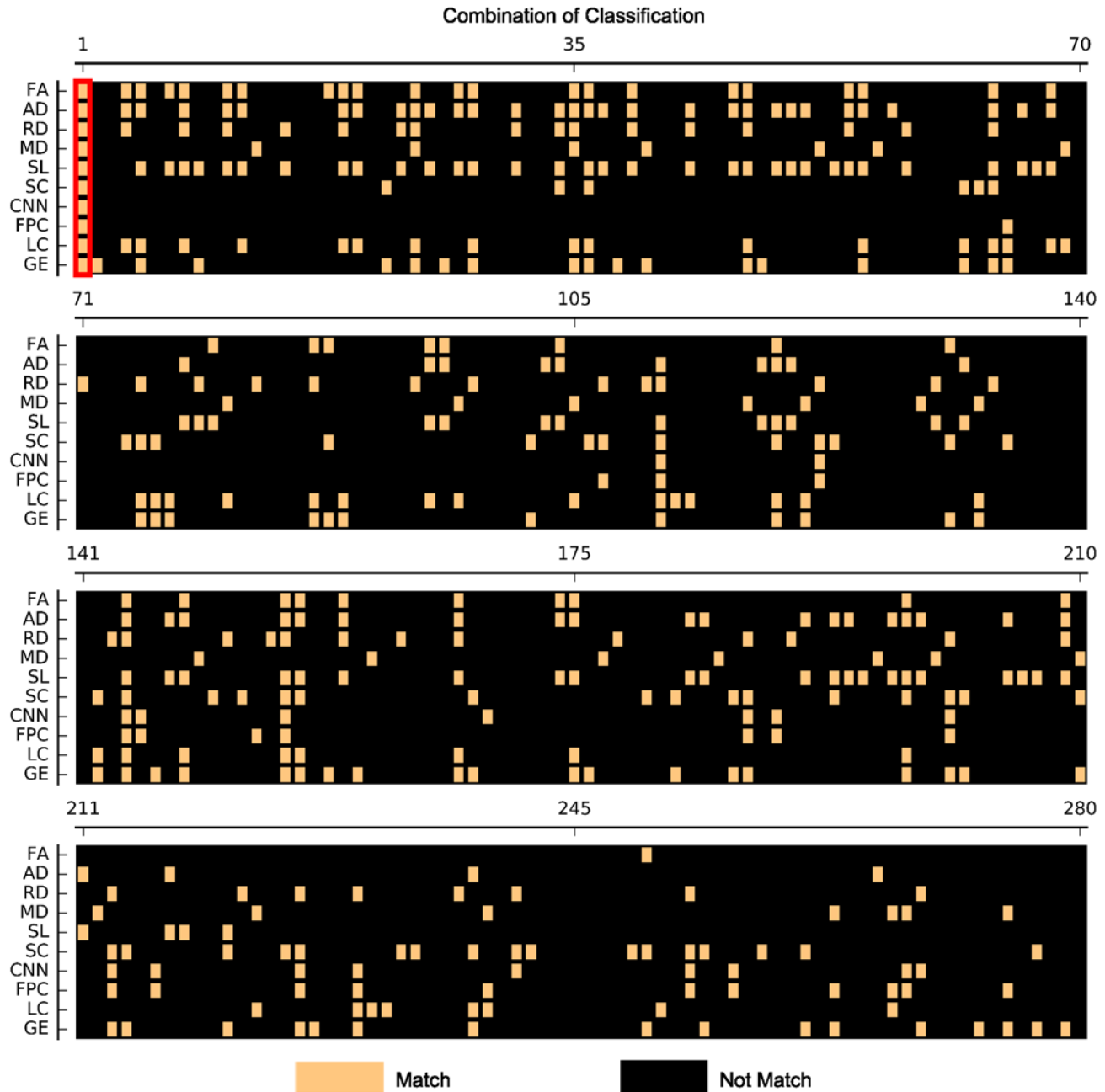


**Figure S3. Consistency of the Miscellaneous Characteristics between All the Possible Surrogate Hubs and Brain Hubs.** The three categories of surrogate hubs were obtained from all the possible combinations of classification with 4, 3 and 1 nodal metrics (1 real combination and 279 surrogate combinations). The statistical comparisons of each characteristic among three categories of hubs were then performed. We next compared the statistical results of each characteristic between brain hubs and surrogate hubs. If it matches we specify it as orange and otherwise black. The first column represents the real combination of the classification of nodal metrics in the brain network.

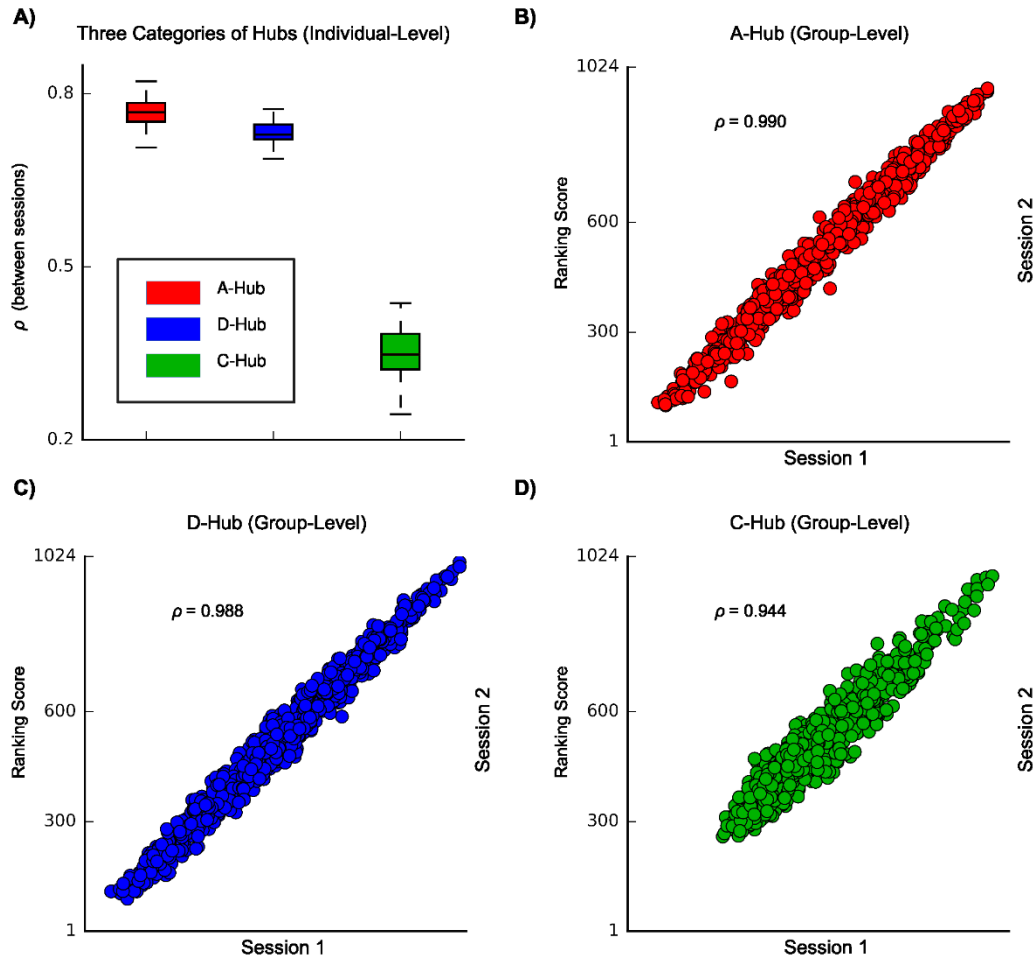


**Figure S4. Spatial Similarities of Hub Indices between Scanning Sessions.** (A) Individual-level spatial correlation. For each box plot, the bottoms and tops of the boxes indicate the first and third quartiles of the Spearman's correlation coefficients across individuals, the band inside the box represents the median, and the whiskers specify the 1.5 interquartile range of the lower and upper quartiles. (B, C, D) Group-level spatial correlations. The red, blue and green plots indicate the aggregated, distributed and connector hub indices, respectively.

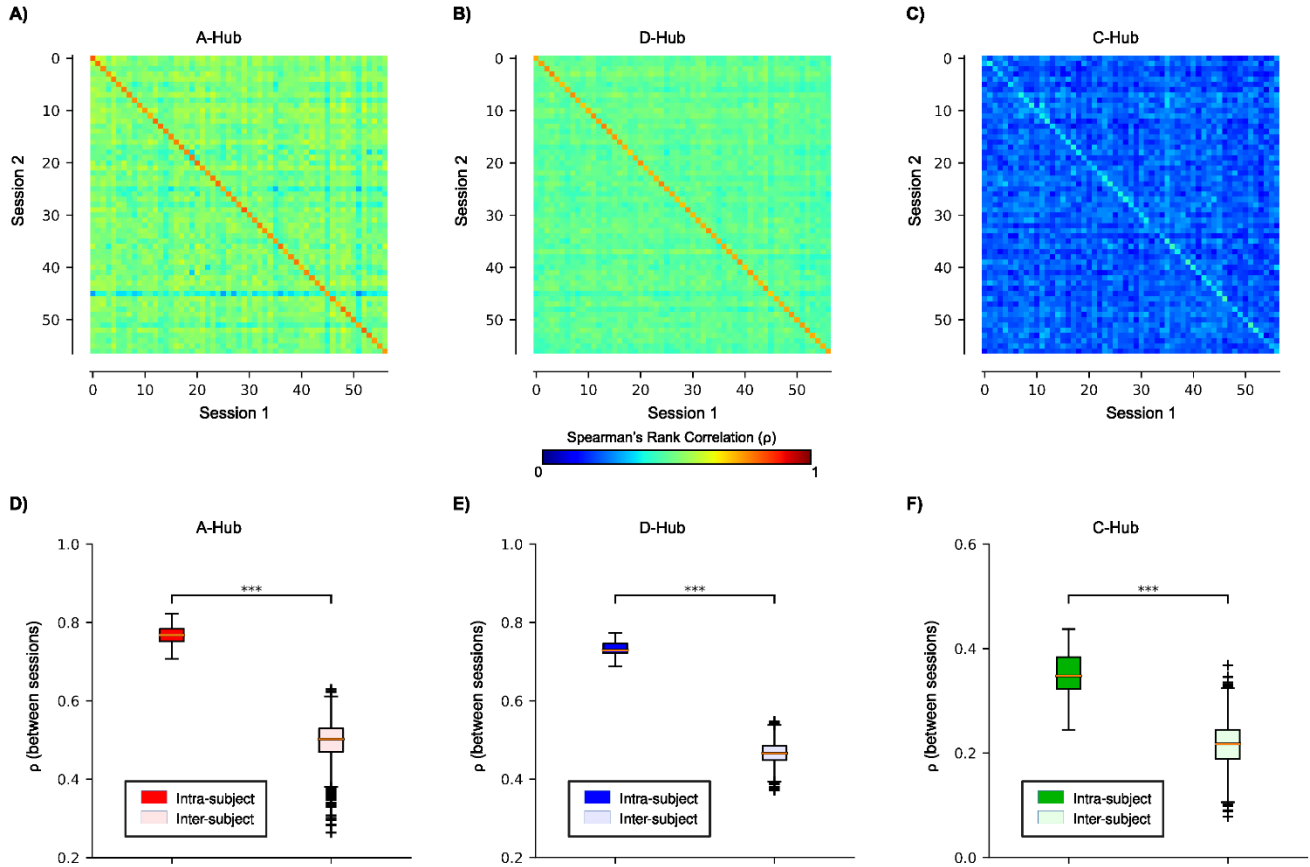


**Figure S5. Intra-subject and Inter-subject variability of three categories of hubs.** (A, B, C) The maps of spatial correlation coefficients among individuals from two scanning sessions. The on-diagonal elements represent intra-subject correlation and the off-diagonal elements specify inter-subject correlation. (D, E, F) The corresponding comparison between intra-subject and inter-subject spatial correlation coefficients. For each box plot, the bottoms and tops of the boxes indicate the first and third quartiles of the Spearman's correlation coefficients, the band inside the box represents the median, and the whiskers specify the 1.5 interquartile range of the lower and upper quartiles. “\*\*\*” represents the significance level ( $P$ -values < 0.001, Bonferroni corrected).

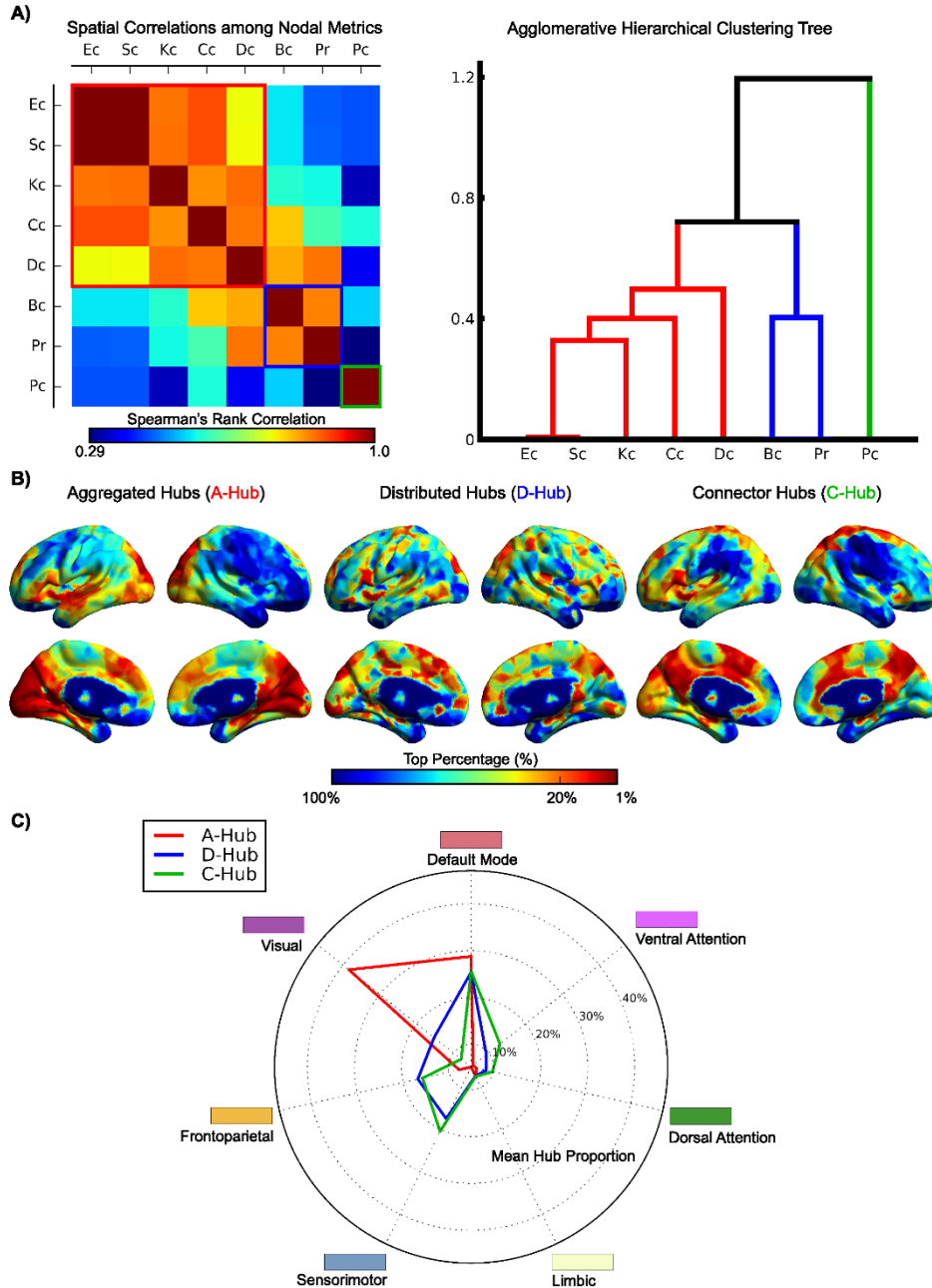


**Figure S6. Identification and Spatial Distribution of the Three Categories of Hubs from Dataset 3.**

(A) The group-averaged map of the Spearman's correlations among the eight nodal metrics and the agglomerative hierarchical clustering tree generated from the map. The red, blue and green solid lines show the classification results, indicating the three categories of metrics used to identify the following aggregated hubs, distributed hubs and connector hubs. (B) Spatial distributions of the three categories of hubs on the brain surface. (C) Spatial distributions of the three categories of hubs in the seven functional systems.

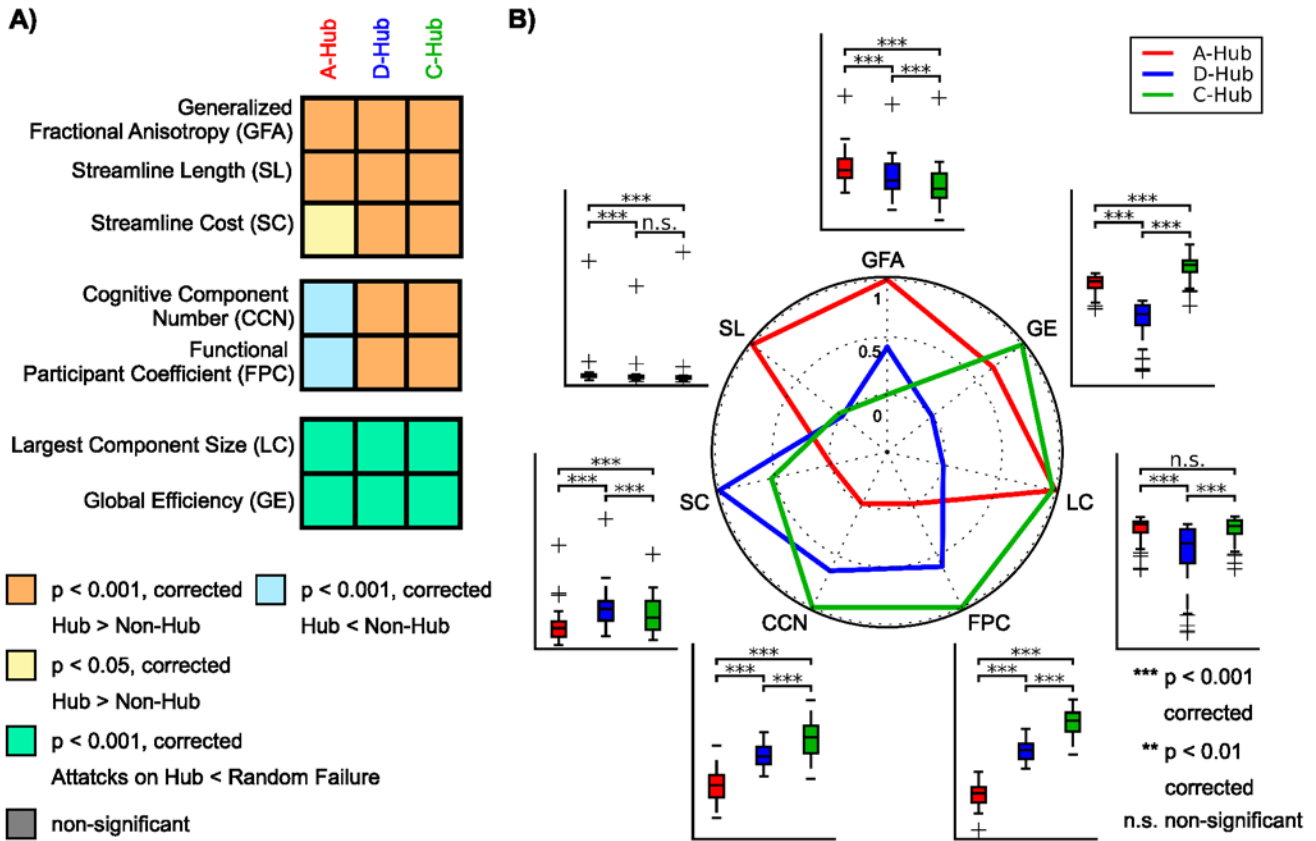


**Figure S7. Miscellaneous Characteristics of the Three Categories of Hubs from Dataset 3.** (A) Comparisons of miscellaneous characteristics between hubs and non-hubs for each category of hubs. (B) Comparisons of these characteristics among the three categories of hubs.

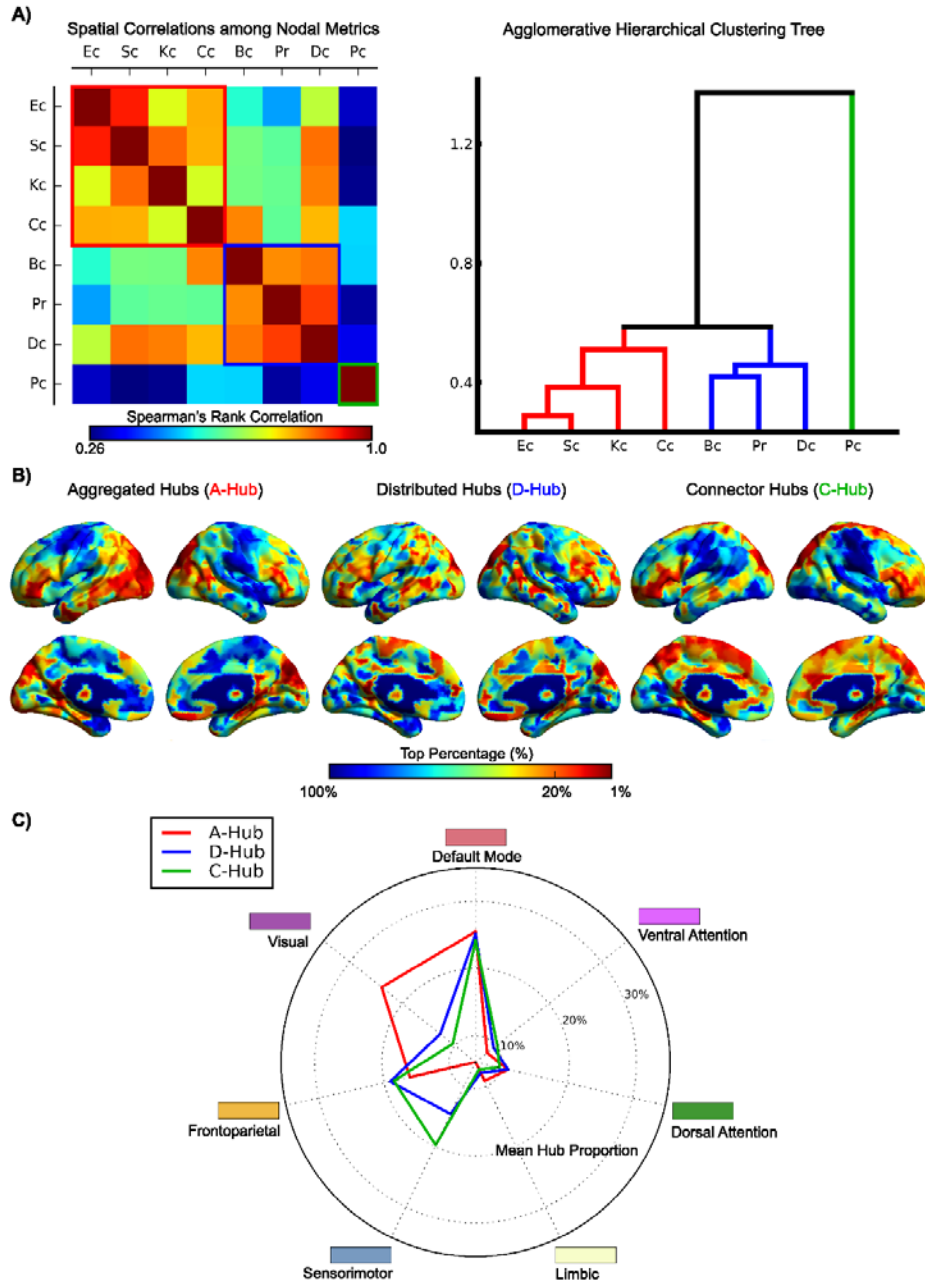


**Figure S8. Identification and Spatial Distribution of the Three Categories of Hubs using the 625-Node Definition.** (A) The group-averaged map of Spearman's correlations among eight nodal metrics and the agglomerative hierarchical clustering tree generated from the map. The red, blue and green solid lines show the classification results, indicating the three categories of metrics used to identify the following aggregated hubs, distributed hubs and connector hubs. (B) Spatial distributions of the three categories of hubs on the brain surface. (C) Spatial distributions of the three categories of hubs in the seven functional systems.

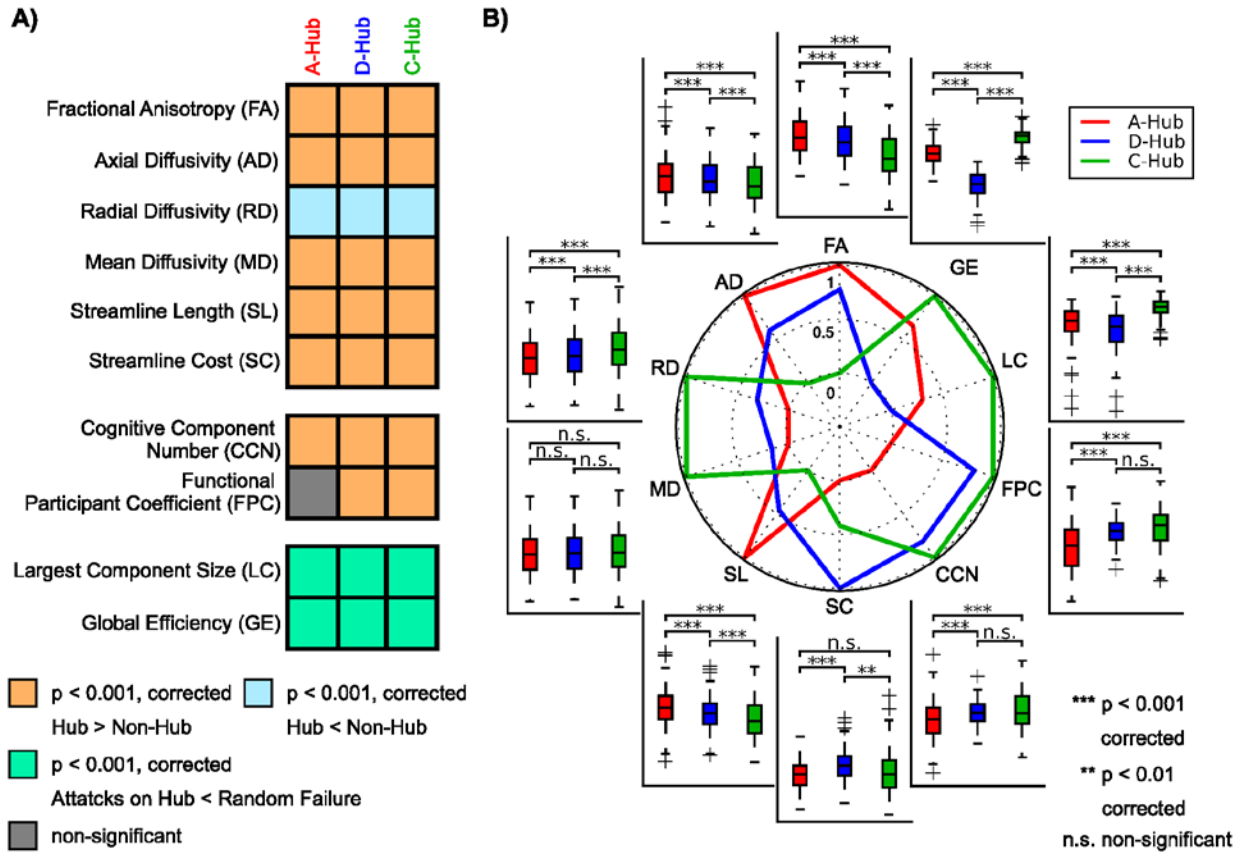


**Figure S9. Miscellaneous Characteristics of the Three Categories of Hubs using the 625-Node Definition.** (A) Comparisons of the miscellaneous characteristics between hubs and non-hubs for each category of hubs. (B) Comparisons of these characteristics among the three categories of hubs.

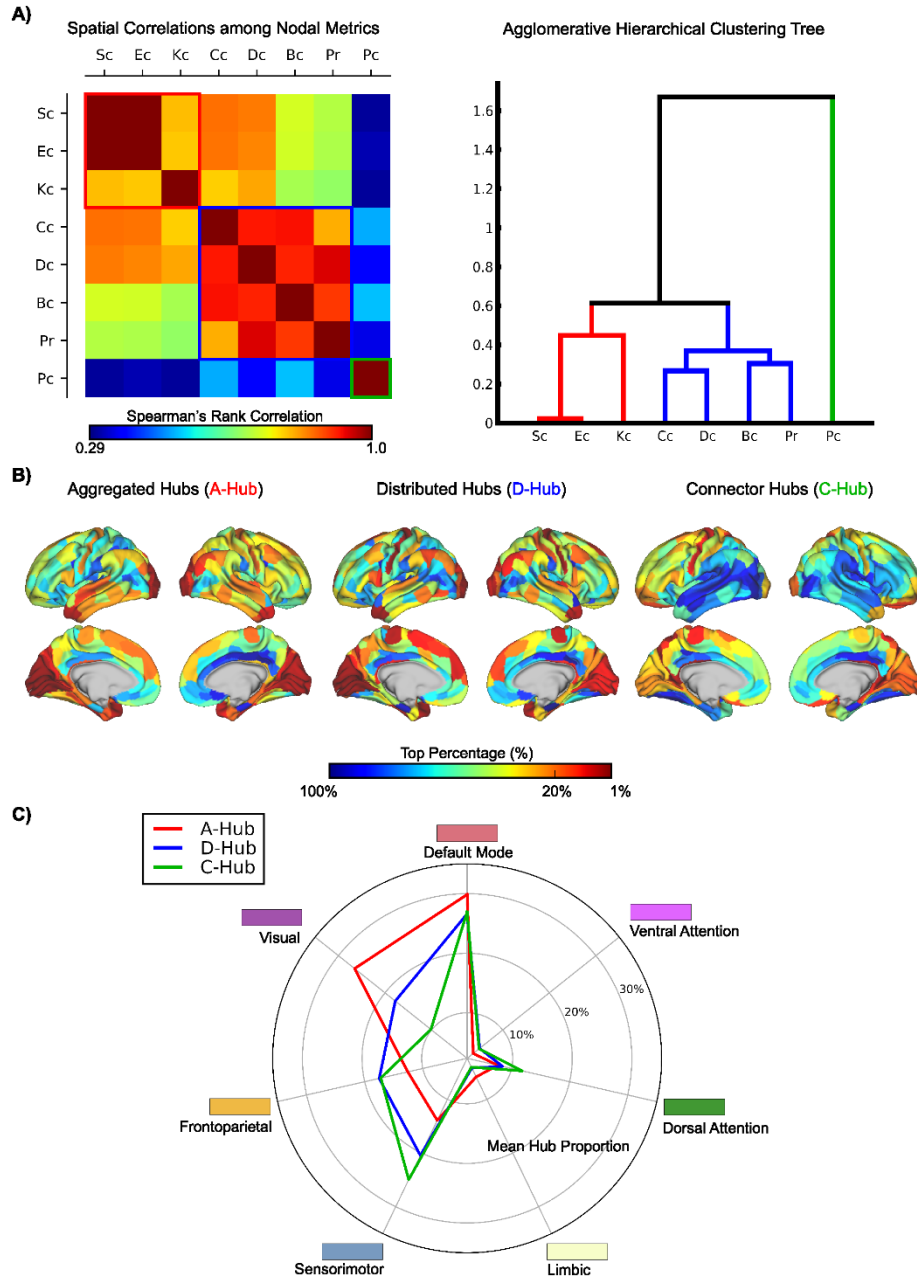


**Figure S10. Identification and Spatial Distribution of the Three Categories of Hubs using the 360-Node Definition.** (A) The group-averaged map of Spearman's correlations among eight nodal metrics and the agglomerative hierarchical clustering tree generated from the map. The red, blue and green solid lines show the classification results, indicating the three categories of metrics used to identify the following aggregated hubs, distributed hubs and connector hubs. (B) Spatial distributions of the three categories of hubs on the brain surface. (C) Spatial distributions of the three categories of hubs in the seven functional systems.

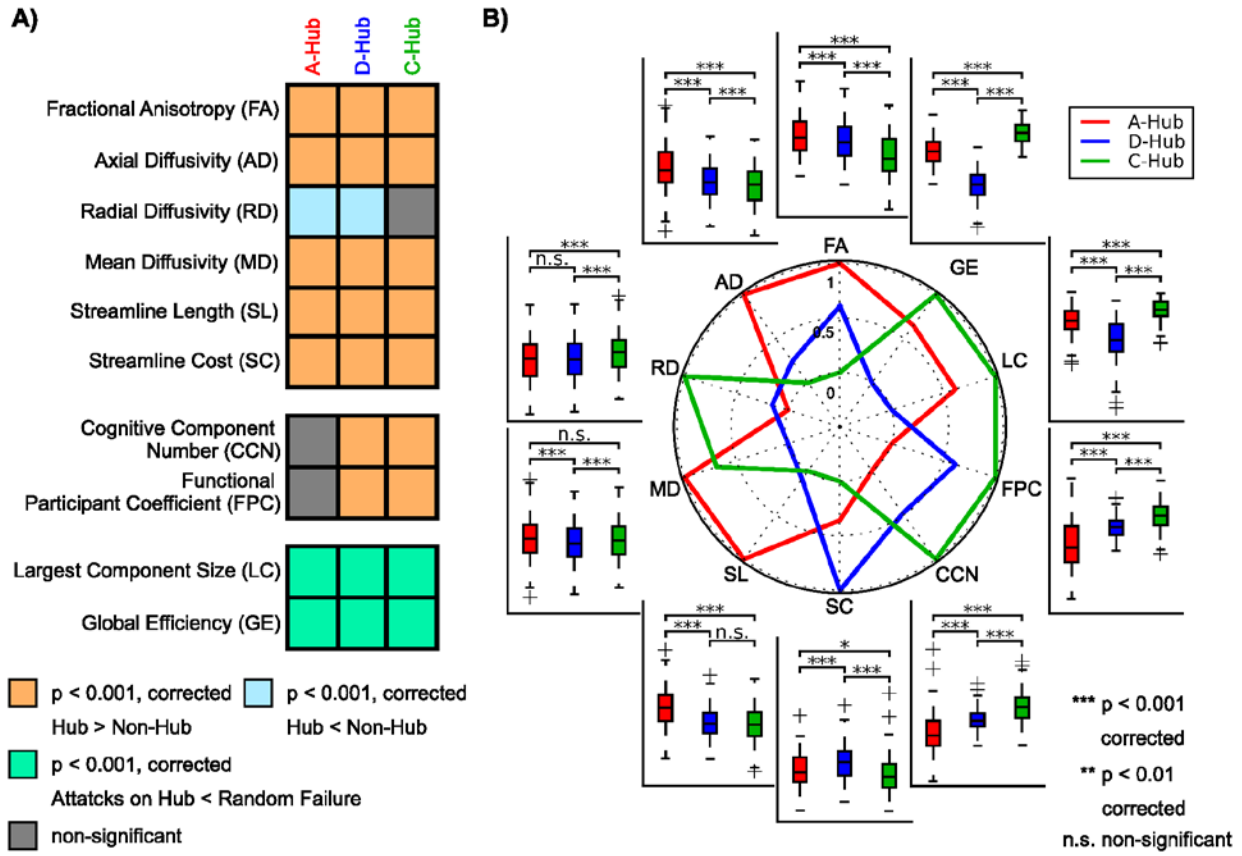


**Figure S11. Miscellaneous Characteristics of the Three Categories of Hubs using the 15% Hub Selective Threshold.** (A) Comparisons of the miscellaneous characteristics between hubs and non-hubs for each category of hubs. (B) Comparisons of these characteristics among the three categories of hubs.

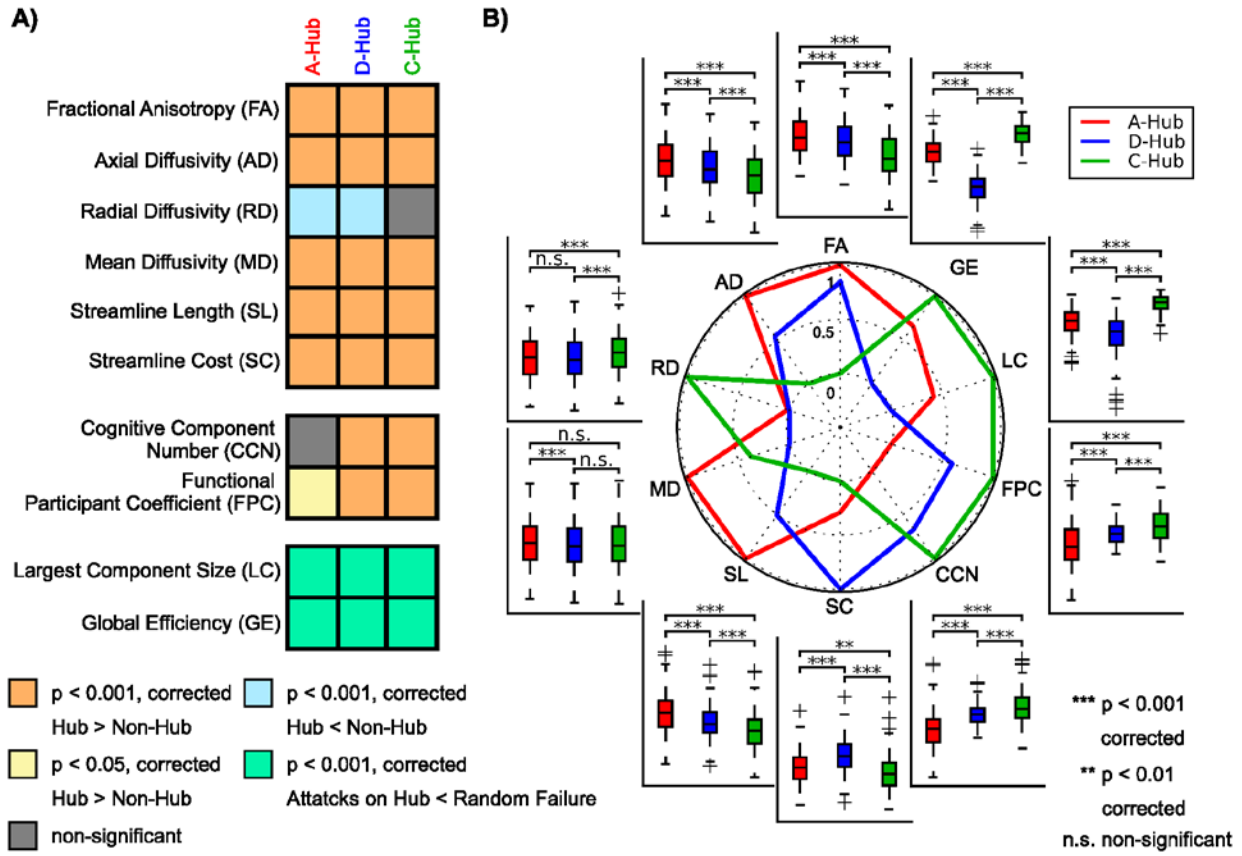


**Figure S12. Miscellaneous Characteristics of the Three Categories of Hubs using the 25% Hub Selective Threshold.** (A) Comparisons of the miscellaneous characteristics between hubs and non-hubs for each category of hubs. (B) Comparisons of these characteristics among the three categories of hubs.

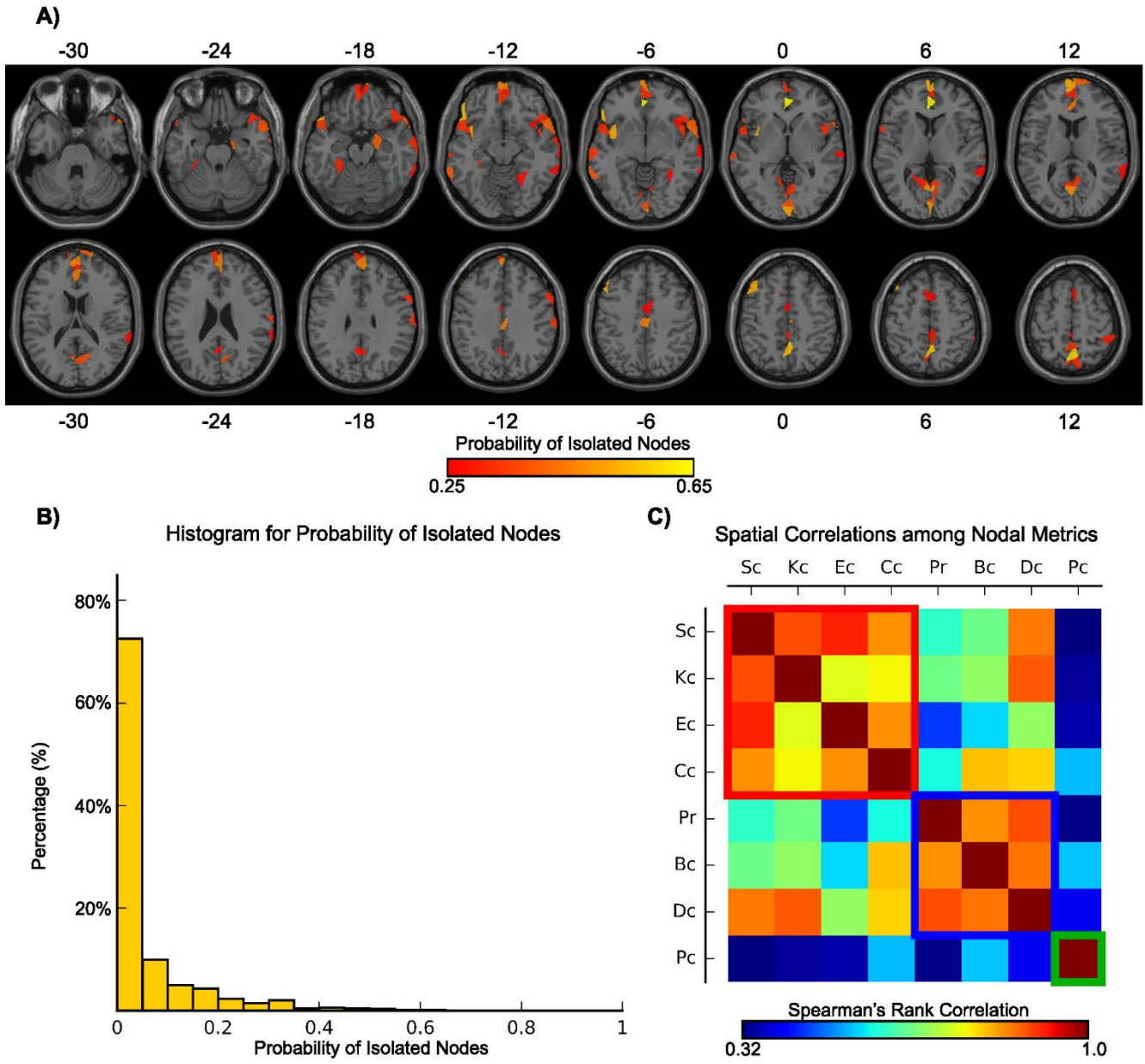


**Figure S13. Spatial Distribution of Isolated Nodes and Identification of Three Categories of Nodal Metrics in the Connected Brain Networks after Removal of Isolated Nodes.** (A) Spatial distribution of isolated nodes (grouped probability > 0.25). (B) Histogram of the probability of isolated nodes across nodes. (C) Identification of nodal metrics with the connected brain networks after removal of isolated nodes.

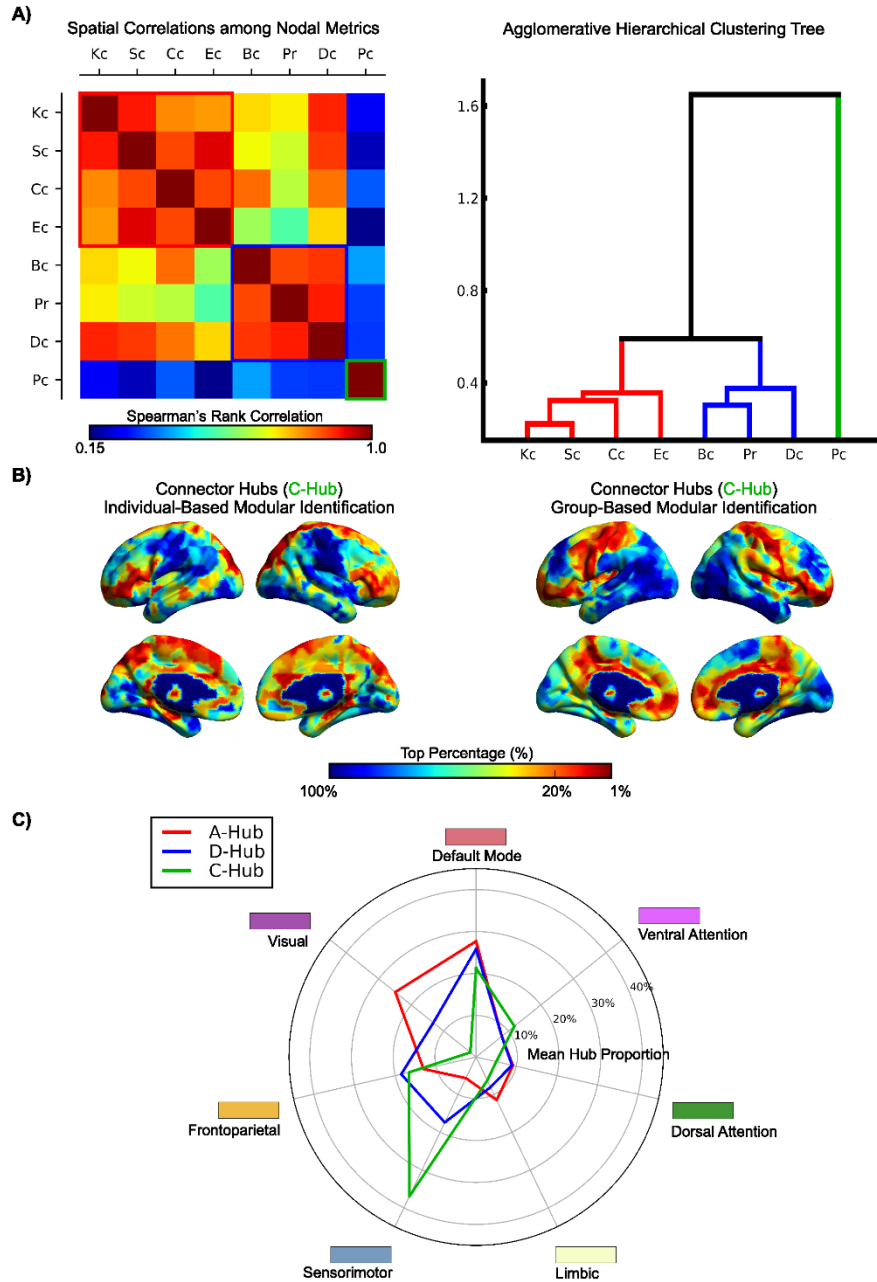


**Figure S14. Identification and Spatial Distribution of the Three Categories of Hubs when the participant coefficient defined by group-level modular organization.** (A) The group-averaged map of Spearman's correlations among eight nodal metrics and the agglomerative hierarchical clustering tree generated from the map. The red, blue and green solid lines show the classification results, indicating the three categories of metrics used to identify the following aggregated hubs, distributed hubs and connector hubs. (B) Left panel: spatial distributions of the connector hubs using individual-level modularity. Right panel: spatial distributions of the connector hubs using individual-level modularity. (C) Spatial distributions of the three categories of hubs in the seven functional systems.

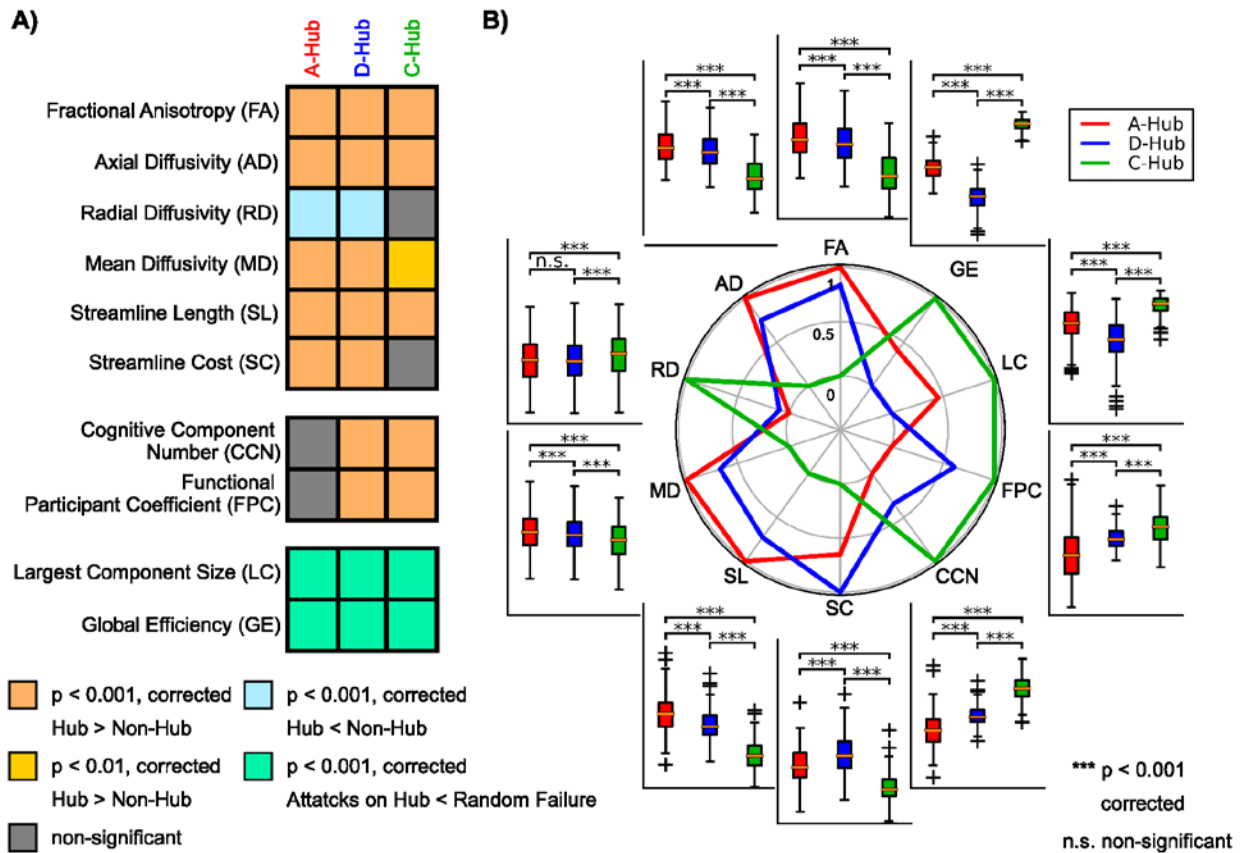


**Figure S15. Miscellaneous Characteristics of the Three Categories of Hubs when the participant coefficient defined by group-level modular organization.** (A) Comparisons of the miscellaneous characteristics between hubs and non-hubs for each category of hubs. (B) Comparisons of these characteristics among the three categories of hubs.